ARTICLE

Mechanism and potential sites of potassium interaction with glutamate transporters

Jiali Wang⬤, Kaiqi Zhang, Puja Goyal, and Christof Grewer⬤

In the mammalian glutamate transporters, countertransported intracellular K^+ is essential for relocating the glutamate binding site to the extracellular side of the membrane. This K^+-dependent process is believed to be rate limiting for the transport cycle. In contrast, extracellular K^+ induces glutamate release upon transporter reversal. Here, we analyzed potential K^+ binding sites using molecular dynamics (MD) simulations and site-directed mutagenesis. Two candidate sites were identified by spontaneous K^+ binding in MD simulations, one site (K1 site) overlapping with the Na1 Na^+ binding site and the K2 site being localized under hairpin loop 2 (HP2). Mutations to conserved amino acid residues in these sites resulted in several transporters that were defective in K^+-induced reverse transport and which bound K^+ with reduced apparent affinity compared with the wild-type transporter. However, external K^+ interaction was abolished in only one mutant transporter $EAAC1_{D454A}$ in the K1 site. Our results, for the first time, directly demonstrate effects of K1-site mutations on K^+ binding, in contrast to previous reports on K^+ binding sites based on indirect evidence. We propose that K^+ binding to the K1 site is responsible for catalyzing the relocation step, whereas binding to the K2 site may have an as-of-yet unidentified regulatory function.

Introduction

Excitatory amino acid transporters (EAATs) from the solute carrier 1 (SLC1) family are an important class of membrane proteins, which are strongly expressed in the mammalian central nervous system, where they are responsible for the transport of glutamate across neuronal and astrocytic membranes. EAATs take up glutamate into cells against a large concentration gradient (Wadiche et al., 1995; Zerangue and Kavanaugh, 1996a), a major function preventing glutamate concentration from reaching neurotoxic levels in the extracellular space (Tanaka et al., 1997; Zerangue and Kavanaugh, 1996a). Dysfunction of glutamate transporter is proposed to be involved in several disorders, including stroke and Alzheimer's disease; however, the exact involvement of EAATs in these diseases is not fully understood. Glutamate transporters take up Na^+, H^+, and glutamate from the extracellular to the intercellular side of the membrane in exchange of one K^+ in the reverse direction (stoichiometry of 3:1:1:1), resulting in a total of two positive charges moving from the outside to the inside of the cell (Wadiche et al., 1995; Zerangue and Kavanaugh, 1996a, 1996b) and, thus, transmembrane current. These ion fluxes are associated with conformational changes of the transporter, leading to alternating access of the glutamate- and ion binding sites.

Currents produced by the transporter are composed of two parts, transport current (stoichiometrically coupled) and anion current (uncoupled; Bergles et al., 2002). While the uncoupled anion current is the most pronounced in the presence of transported substrates, smaller anion current is also observed without substrate, which is termed the leak current (Wadiche et al., 1995). Anion current is induced as the transporter transitions through specific states in the transport cycle (Machtens et al., 2015), the most prominent one likely being an intermediate state between outward-facing and inward-facing conformations (Verdon and Boudker, 2012). K^+-induced anion currents are much lower than those in the presence of Na^+ (Zhang et al., 2007).

Several crystal structures of the archaeal (Glt_{Ph}), bacterial, and a mammalian glutamate transporter have been published (Boudker et al., 2007; Canul-Tec et al., 2017; Guskov et al., 2016; Reyes et al., 2009; Verdon and Boudker, 2012; Yernool et al., 2004), providing information about the elevator-based alternating access transport mechanism and allowing the direct identification of the substrate binding site and two Na^+-binding sites (Na1 and Na2). Together with the archaeal glutamate transporter Glt_{Tk} (Guskov et al., 2016) homologue structure,

electrophysiological and computational studies on mammalian transporters, a third Na$^+$ binding site (Na3) was proposed, in proximity to the highly conserved D367 side chain in transmembrane domain 7 (TM7; Bastug et al., 2012; Tao et al., 2006, 2010), excitatory amino acid carrier 1 (EAAC1) numbering (EAAC1 is the rat analogue of human EAAT3). In addition, results from site-directed mutagenesis suggested that the E373 carboxylate side chain is a key player in protonation of the transporter (Grewer et al., 2003; Heinzelmann and Kuyucak, 2014). The substrate binding site is highly conserved in EAATs and includes the R446 side chain, which is responsible for coordination of the negatively charged γ-carboxylate group of glutamate (Bendahan et al., 2000). Finally, two highly conserved hairpin loops (HP1 and HP2) were proposed to provide a gate function associated with substrate binding and release (Boudker et al., 2007; Yernool et al., 2004). However, more recent structures based on Glt$_{Tk}$ and the glutamine transporter alanine serine cysteine transporter 2, which is also an SLC1 member, suggest a one-gate mechanism, in which HP2 serves as the gate in both outward-facing and inward-facing configurations (Arkhipova et al., 2020; Garaeva et al., 2019; Zomot and Bahar, 2013).

In contrast to glutamate and Na$^+$ binding sites, much less is known about the location of the K$^+$ binding site and the mechanism of K$^+$ interaction with the transporter. In the mammalian glutamate transporters, but not in Glt$_{Ph}$, K$^+$ binding and relocation are necessary steps in glutamate transport, ensuring that the glutamate binding site becomes exposed to the extracellular side after the transport cycle is complete (Kanner and Bendahan, 1982). This K$^+$-dependent relocation process is believed to be electrogenic and a rate-limiting step in the transport cycle (Grewer et al., 2000). In several site-directed mutagenesis studies, effects of mutations on K$^+$ interaction with the transporter were tested. It was suggested that E373 is involved in K$^+$-induced transporter relocation (Kavanaugh et al., 1997), potentially creating a binding pocket for K$^+$, as predicted from an apo-Glt$_{Tk}$ structure (Jensen et al., 2013). However, a report based on site-directed mutagenesis data showed that the E373Q mutation did not abolish K$^+$ binding (Grewer et al., 2003). In addition, the T387P mutation (hEAAT1 numbering) abolishes K$^+$-induced transporter relocation (Kovermann et al., 2017). Furthermore, Na$^+$ binding sites (Heinzelmann et al., 2011; Holley and Kavanaugh, 2009; Teichman et al., 2009) and the substrate binding site (Holley and Kavanaugh, 2009; Verdon et al., 2014) were proposed to form overlapping K$^+$ binding sites.

In this work, we observed spontaneous binding of K$^+$ in MD simulations to two potential binding sites, K1 and K2. Amino acid residues predicted to contribute to these binding sites were tested using site-directed mutagenesis. While many of the mutations interfere with K$^+$-induced reverse transport, only one mutation, D454A in the K1 site, was found to abolish external K$^+$ association with the transporter. Together, our data provide the first direct functional evidence for the K1–K$^+$ binding site, which overlaps with the Na1 site. Occupancy of this site is proposed to be necessary for relocation. In addition, our results further raise the possibility of another possibly regulatory K$^+$ binding site (K2), which is enclosed by HP2.

Materials and methods

Cell culture and transfection

HEK293 cells (American Type Culture Collection; no. CRL 1573) were cultured as described previously (Wang et al., 2018). Cell cultures were transiently transfected with wild-type or mutant EAAC1 cDNAs, inserted into a modified pBK-cytomegalovirus expression plasmid (pBK-CMV), using Jetprime transfection reagent according to the protocol supplied by the manufacturer (Polyplus). The cells were used for electrophysiological measurements between 24 and 36 h after transfection. All data are shown as mean ± SD, collected from >8–10 cell recordings.

Electrophysiology

Currents associated with glutamate transporters were measured in the whole-cell current recording configuration. Whole-cell currents were recorded with an EPC7 patch-clamp amplifier (ALA Scientific) under voltage-clamp conditions. The resistance of the recording electrode was 3–6 MΩ. Series resistance was not compensated because of the small whole-cell currents carried by EAAC1. The composition of the solutions for measuring forward transport currents was 140 mM NaMes (Mes, methanesulfonate), 2 mM MgGluconate$_2$, 2 mM CaMes$_2$, 10 mM HEPES, and 10 mM glutamate, pH 7.3 (extracellular); and 130 mM KMes, 2 mM MgGluconate$_2$, 5 mM EGTA, and 10 mM HEPES, pH 7.3 (intracellular), as published previously (Wang et al., 2018). For anion current recordings, intracellular Mes$^-$ was replaced by thiocyanate (SCN$^-$). For reverse transport current recordings, KMes was used as external solution, and 130 mM NaMes and 5 mM glutamate were used as internal solution. In leak current experiments, we use 130 mM NaSCN solution as intracellular solution without glutamate.
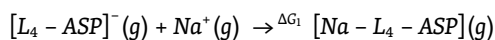
MD simulations

The model system for MD simulations was generated with VMD (Visual Molecular Dynamics) software (Humphrey et al., 1996) using an EAAT3 homology model based on the EAAT1 (PDB accession no. 5LM4; Canul-Tec et al., 2017) and Glt$_{Ph}$ (PDB accession no. 2NWX; Boudker et al., 2007) structures built using HHpred and Modeller from the MPI Bioinformatics Toolkit (Zimmermann et al., 2018) website (sequence alignment shown in Fig. S1). For the EAAT3-Glt$_{Ph}$ homology model, total structure backbone RMSD with respect to the template is 1.4 Å, and for the transport domain backbone, RMSD is 1.04 Å. This is expected, because the transport domain shows the highest percentage of conservation between the two transporters. We also used the structure of EAAT1 (PDB accession no. 5LM4) for simulations (Canul-Tec et al., 2017). In the final EAAT3 homology model, the apo subunit structure was used for the K$^+$ binding simulations. To test quality of the model, we used QMEANBrane for quality check of membrane proteins. The z-scores were EAAT1, 0.52; EAAT3 based on EAAT1, 0.51; Glt$_{Ph}$, 0.65; and EAAT3 based on Glt$_{Ph}$, 0.44. These z-scores are all in the same range and fall into the "good model" category, close to native structures. Medium-quality or poor models are expected to have negative z-scores (Studer et al., 2014). The EAAT3 homology model with Na$^+$/Asp bound was inserted in a preequilibrated POPC lipid bilayer with the dimensions ~130 × 130 Å. TIP3P water was added to generate

a box measuring ~100 Å in the z-direction. NAMD (Phillips et al., 2005) simulations were performed using 2,000 steps of minimization, followed by up to 5-ns equilibration runs under constant pressure conditions (NPT; isothermal-isobaric ensemble), and then switched to the ACEMD (Harvey et al., 2009) program for longer production runs (NVT; canonical ensemble). Na$^+$/Asp was then removed, and the model was allowed to equilibrate for 120 ns, after which the RMSD was in steady state (see Fig. S4). KCl was then added at a total concentration of 0.5, 1, or 2 M, and the system was neutralized using Cl$^-$ as the counter ion. The total numbers of atoms in the EAAT3 system were 139,958 (Glt$_{Ph}$ based) and 213,341 (EAAT1 based). Simulations were run using the CHARMM36 force field and NAMD (Phillips et al., 2005). The RMSD increased slightly after K$^+$ addition, probably due to a slight change in structure induced by cation binding (see Fig. S4). In NAMD simulations, the cutoff for local electrostatic and van der Waals interactions was set to 12 Å. For long-range electrostatic interactions, we used the particle-mesh Ewald method implemented in NAMD. Bonds to hydrogen atoms and TIP3P water were kept rigid using SHAKE. The time steps of the simulations were 2 fs. For ACEMD simulation, the cutoff for short-range interactions was 9 Å (Zielewicz et al., 2019). The complete simulation system, including substrate, lipid, and water, is shown in Fig. S2.
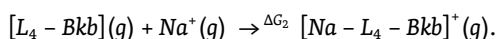
Quantum mechanical (QM) calculations

The gas-phase model systems were built on the basis of the EAAT3 homologue structure in the Na$^+$ binding state. The side chains of D454, S332, and N365, in addition to the main-chain carbonyls of N451 and G361, were considered as the ligands in the K1/Na1 site. As described in Dudev et al. (2018), N-methylacetamide (CH$_3$CONHCH$_3$, Bkb) was used to model the backbone peptide group as well as the Asn/Gln side chain. Ser/Thr and Asp/Glu side chains were modeled as ethanol (CH$_3$CH$_2$OH) and acetate (CH$_3$COO$^-$), respectively. All ligand modifications were done using Avogadro (Hanwell et al., 2012) and the VMD program (Humphrey et al., 1996). Geometry optimization on the models was performed using B3LYP/6-31+G(3d,p) and the Gaussian 09 electronic structure program (Frisch, 2016).
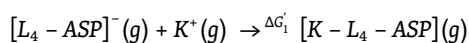
Representing $[(Bkb)_3 - SER]$ as L_4, and considering the binding processes below, the effect of Asp to Asn (Bkb) mutation on Na$^+$ binding is given by $\Delta\Delta G_{Na^+} = (\Delta G_2 - \Delta G_1)$:
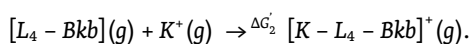
$$[L_4 - ASP]^-(g) + Na^+(g) \xrightarrow{\Delta G_1} [Na - L_4 - ASP](g)$$

and

$$[L_4 - Bkb](g) + Na^+(g) \xrightarrow{\Delta G_2} [Na - L_4 - Bkb]^+(g).$$

Similarly, the effect of Asp to Asn (Bkb) mutation on K$^+$ binding is given by $\Delta\Delta G_{K^+} = (\Delta G_2' - \Delta G_1')$, where $\Delta G_1'$ and $\Delta G_2'$ are the free energy changes of the processes below:

$$[L_4 - ASP]^-(g) + K^+(g) \xrightarrow{\Delta G_1'} [K - L_4 - ASP](g)$$

and

$$[L_4 - Bkb](g) + K^+(g) \xrightarrow{\Delta G_2'} [K - L_4 - Bkb]^+(g).$$

The difference between $\Delta\Delta G_{Na^+}$ and $\Delta\Delta G_{K^+}$ can be computed using the following expression:

$$\Delta\Delta\Delta G = \Delta\Delta G_{Na^+} - \Delta\Delta G_{K^+} =$$
$$G_{[Na-L_4-Bkb](g)} - G_{[Na-L_4-ASP](g)} + G_{[K-L_4-ASP](g)} - G_{[K-L_4-Bkb](g)}.$$

Thermochemical data were calculated at T = 298.15 K, and the calculated free energies of gas-phase complexes included zero-point energy and entropic contributions. ΔG_2 and $\Delta G_2'$ are larger than ΔG_1 and $\Delta G_1'$, respectively, since the former are the binding free energies after the neutralization of the negative charge of Asp. Hence, $\Delta\Delta\Delta G > 0$ or $(\Delta G_2 - \Delta G_1) > (\Delta G_2' - \Delta G_1')$ implies that Na$^+$ binding is weakened more than K$^+$ binding due to the Asp to Asn mutation in the gas phase.

Immunofluorescence

Immunostaining of EAAC1-expressing cells was performed as described (Tao and Grewer, 2005). In brief, transfected HEK293 cells, plated on poly-D-lysine–coated coverslips, were fixed in 5% acetic acid in methanol for 4 min at –20°C. After several washing steps with PBS, they were incubated overnight at 4°C in 0.1% (vol/vol) Triton X-100 in PBS in the presence of 0.01 mg/ml affinity-purified EAAC1 antibody (Alpha Diagnostics). Following primary antibody incubation, the cells were rinsed and incubated (1 h) with anti-rabbit IgG conjugated to Cy3 (1:500; Dianova) in PBS containing 0.1% (vol/vol) Triton X-100. After washing with PBS and water, the cells were coverslipped in Mowiol (Hoechst). The Cy3 immunofluorescence was excited with a mercury lamp, visualized with an inverted microscope (Zeiss) using a TMR filter set (Omega) and photographed with a digital camera (Sony).

Online supplemental material

Fig. S1 shows the sequence alignment used for generating the EAAT3 homology model, in analogy to alignments presented by Yernool et al. (2004). Fig. S2 shows the simulation environment. Fig. S3 shows MD simulations revealing potential K$^+$ binding sites in EAAT1. Fig. S4 shows typical RMSD plots for MD simulations before and after application of high [K$^+$], showing that the *apo* structure was equilibrated. Fig. S5 shows K$^+$ radial distribution functions from spontaneous K$^+$ binding simulations. Fig. S6 shows EAAC1 WT and mutant expression tested using immunofluorescence microscopy. Table S1 shows an EAAT3 homology model based on Glt$_{Ph}$. Table S2 shows distances between the central metal ion and ligands in the quantum-mechanically optimized structures of the gas-phase models.

Results

Two potential K$^+$ binding sites revealed by MD simulations

To identify potential glutamate transporter K$^+$ binding sites, we tested whether spontaneous K$^+$ binding can be observed in MD simulations. For this purpose, we selected the outward-facing transporter in the *apo* state (no glutamate or cations bound), based on EAAT3 homology models of Glt$_{Ph}$ (Boudker et al., 2007), which shares 37% sequence identity and 55% similarity with EAAT3 (Yernool et al., 2004). EAAT3 was used because, in our hands, its rat analogue, EAAC1, generates larger transport and anion currents than EAAT1 and EAAT2 (in HEK293 cells)
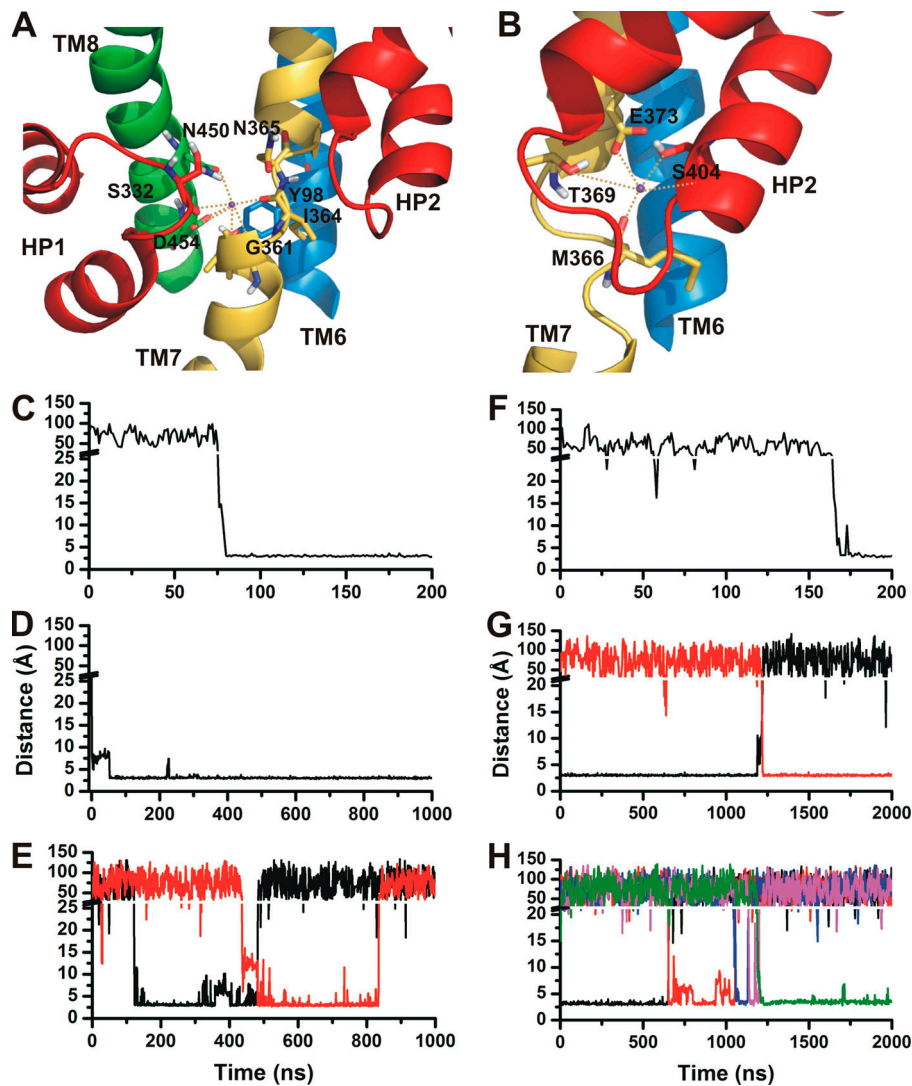
Figure 1. **Spontaneous K⁺ binding in MD simulations reveals two potential K⁺ binding states.** MD simulation results are based on an EAAT3 homology model (Glt$_{Ph}$ template). Typical trajectories from microsecond-timescale simulations are selected and analyzed. **(A–H)** Binding state with K⁺ located close to the side chain of D454 (K1 site; A) and K⁺ located close to the side chain of E373 (K2 site; B). Trajectories from independent simulations demonstrating spontaneous K⁺ binding to K1 (C–E) and K2 (F–H) sites were analyzed. The colors represent different K⁺ ions. The binding of K⁺ to the K1 site was monitored by the distance between K⁺ and the C$_\gamma$ atom of D454, while the binding of K⁺ to the K2 site was monitored by the distance between K⁺ and the C$_\delta$ atom of E373. The K⁺ concentration was 1 M.

and is thus more amenable to analysis of mutant transporters (see below). As controls, we also performed MD simulations with the EAAT1 crystal structure and an EAAT3 homology model based on the EAAT1 structure (Canul-Tec et al., 2017). In all structures, aspartate and the Na⁺ ions were removed before adding K⁺ to the solutions, after which the simulations were run with harmonic constraints for 5 ns, before unconstrained runs. To increase the likelihood of observing spontaneous binding events within the MD simulation timescale (1–2 µs), we performed the simulations in 0.5, 1.0, and 2.0 M KCl. Under such supersaturated concentration conditions, cation-binding processes are expected to be accelerated by increasing binding probability, as previously demonstrated for anion association with glutamate transporters (Machtens et al., 2015).

In 20 µs-level MD simulations (Table S1), spontaneous K⁺ binding was observed to two binding sites, one overlapping with the Na1 (Boudker et al., 2007) site (K1; Fig. 1 A) and the other close to the substrate binding site (Holley and Kavanaugh, 2009), covered by the HP2 loop (K2; Fig. 1 B). In the potential K1 site shown in Fig. 1 A, side chains of amino acid residues from HP1, TM7, TM8, D454, S332, and N365 contribute to K⁺

coordination, in addition to the main-chain carbonyls of N451 and G361. D454 is predicted to contribute both side-chain oxygen atoms as ligands to the binding site, as seen in Na⁺-bound structures (Boudker et al., 2007), consistent with a total of six ligands for K⁺ coordination. Water oxygen was present at 2.8–2.9 Å distance from K⁺ at 35% of the time and thus may also contribute to coordination. At the K2 site, side chains of amino acids in TM7, E373, and T369 are predicted to contribute to K⁺ coordination, as well as S404 in HP2. Finally, the main-chain carbonyl from M366 is involved. All of these residues are highly conserved within the mammalian glutamate transporters EAAT1–EAAT5, but E373 is not conserved in the neutral amino acid transporter members of the SLC1 family and Glt$_{Ph}$, which do not require K⁺ for transport. Kortzak et al. (2019) suggested that K⁺ can, however, bind to Glt$_{Ph}$, using a fluorescence microscale thermophoresis assay, although the fluorescence changes were small and occurred at high K⁺ concentrations. In contrast to mammalian EAATs, Glt$_{Ph}$ can relocate the substrate-binding site in the absence of K⁺, providing an explanation as to why K⁺ is not required for Glt$_{Ph}$ turnover, although the K1 site is very similar in both mammalian EAATs and Glt$_{Ph}$.

Wang et al.
K⁺ interaction with glutamate transporters

Journal of General Physiology   4 of 12
https://doi.org/10.1085/jgp.202012577

In our EAAT3 *apo* homology model, the side chain of M366 (analogous to M311, Glt_Ph) is pointed away from the substrate binding site, as is the case in *apo* Glt_Ph and Glt_Tk (Jensen et al., 2013; Verdon et al., 2014). This position of M366, facing away from the substrate binding site, remains in the predicted K$^+$-bound state (K1-site; Fig. 1 A). However, in contrast to the substrate/Na$^+$-bound state, in which the M366 side chain points toward the substrate binding site (Jensen et al., 2013; Verdon et al., 2014), the backbone carbonyl of N365 (analogous to N310 in Glt_Ph) is able to contribute as a ligand to the K$^+$ binding site, possibly because of the larger diameter of the K$^+$ ion compared with Na$^+$. This is an interesting finding, because the structural basis of relocation in the unwound region of TM7 appears to be conserved between EAAT3 and Glt_Ph, despite the difference in the requirement of K$^+$ for relocation in the two transporters.

Control MD simulations performed with EAAT1 and with an EAAT3 homology model based on the EAAT1 crystal structure (Canul-Tec et al., 2017), with which EAAT3 shares much higher sequence identity and similarity (54% and 69%, respectively; Yernool et al., 2004) than with Glt_Ph, also showed spontaneous K$^+$ binding to the same K$^+$ binding sites (Fig. S3). The amino acid residues providing ligands to the K$^+$ binding sites were conserved in the EAAT1 simulations (Fig. S3) and the EAAT3 homology models (Fig. 1). K$^+$ binding to the K2-site required deprotonation of E373 (Table S1), which was previously predicted to be the proton acceptor of EAAT3 (Grewer et al., 2003). These results suggest that spontaneous K$^+$ binding was not artificially caused by the use of a homology model.

Sample trajectories of the K$^+$-binding events are shown in Fig. 1, C–H (distance between K$^+$ and reference residues is plotted on the y axis). K$^+$ typically spontaneously associated with the transporter within <150 ns at the K1 site (Fig. 1 C), and residency times, once bound, were for most simulations >300 ns (Fig. 1, D and E; and Table S1). In 22 trajectories, multiple K$^+$ association/dissociation events were observed. Similar results were found for the K2 site (Fig. 1, F–H); however, rebinding of K$^+$ was faster than at the K1 site, possibly due to the better accessibility from the extracellular solution. We also tested spontaneous K$^+$ association under a condition of mixed, equal K$^+$/Na$^+$ concentrations (0.5 M each; data not shown). The data were similar to the K$^+$-only simulations. These results indicate that the two binding sites have preference for K$^+$ over Na$^+$ ions. The RMSD versus time plot and radial distribution function analysis of K$^+$ binding are shown in Fig. S4 and Fig. S5.

K$^+$-induced reverse transport is inhibited in transporters with mutations to the potential K$^+$ binding sites

K$^+$-induced relocation is an important step in the glutamate transport cycle. Under forward transport conditions, intracellular K$^+$ catalyzes this relocation reaction to expose glutamate binding sites to the extracellular side. Here, we used application of extracellular K$^+$ in the reverse transport mode (in the presence of intracellular Na$^+$ and glutamate) to test the effect of mutations on transport and relocation in the reverse direction. In Fig. 2 A, a typical steady-state reverse transport current recorded from EAAC1_WT-expressing cells is shown. As expected

(Kanner and Bendahan, 1982; Kavanaugh et al., 1997; Szatkowski et al., 1990; Wang et al., 2019; Zhang et al., 2007), this current is outwardly directed due to the coupled outward movement of two positive charges for each K$^+$ ion taken up. The outward currents were dependent on K$^+$ concentration, as reported previously (Wang et al., 2019; data not shown). Next, we recorded K$^+$-induced reverse transport currents from 15 transporters with mutations to amino acids directly contributing to the predicted K$^+$ binding sites or close to those sites. These were characterized as K1 site, K2 site, Na3 site, or other mutations. Representative current recordings for EAAC1_Y98F and EAAC1_D454N are shown in Fig. 2 B. Y98 is close to the K1 site but is not predicted to contribute a ligand to it, whereas the D454 side chain contributes both side-chain oxygens to the site. Consistently, the Y98A mutation did not inhibit K$^+$-induced reverse transport current, whereas the D454N mutation did. Overall, three transporters with mutations in positions Y98 (A and F) and T363 (A) retained significant reverse transport activity, and the other mutant transporters showed significantly reduced reverse transport current of ≤82% of wild-type transporter (Fig. 2 C). For the K2 site, all mutations significantly reduced K$^+$-induced reverse transport activity, but only mutations to one site (E373) virtually abolished it (Fig. 2 C). A transporter with the K2-site M366A mutation was also studied but showed too little activity to be analyzed quantitatively.

In addition, we found that EAAC1_WT, as well as EAAC1_D454N, displayed a noticeable transient outward current after K$^+$ application through rapid solution exchange (Fig. 3, A and B). Notably, similar transient currents, which were, however, smaller in magnitude than the wild-type current, were also obtained with E373Q, D444N mutant transporters (Fig. 3 B). In previous reports (Grewer et al., 2012; Kortzak et al., 2019), similar outward transient currents were attributed to reactions associated with the K$^+$-induced relocation reaction (Fig. 3 C). Together, these results indicate that most of the mutations made to conserved residues contributing to cation binding sites severely impair reverse transport function in the presence of external K$^+$.

The possibility has to be considered that certain mutations prevent expression of the transporter in the membrane rather than reverse transport, which would also give rise to a lack of reverse transport current. To test this possibility, we performed immunostaining for all mutant transporters tested here. As shown in Fig. S6, immunofluorescence was observed in all mutant transporters, indicating membraneous localization due to fluorescence observed at the cell borders. In contrast, control, nontransfected cells did not show immunofluorescence.

Effects of Na/K-site mutations on Na$^+$/glutamate homoexchange and glutamate binding

In the presence of Na$^+$/glutamate on both sides of the membrane, the transporter is locked in the homoexchange mode. Because the presence of K$^+$ is not necessary to establish the homoexchange mode, in which amino acid substrate is exchanged across the membrane without net substrate transport, we tested the effect of potential cation-site mutations on exchange current. Typical anion current upon application of
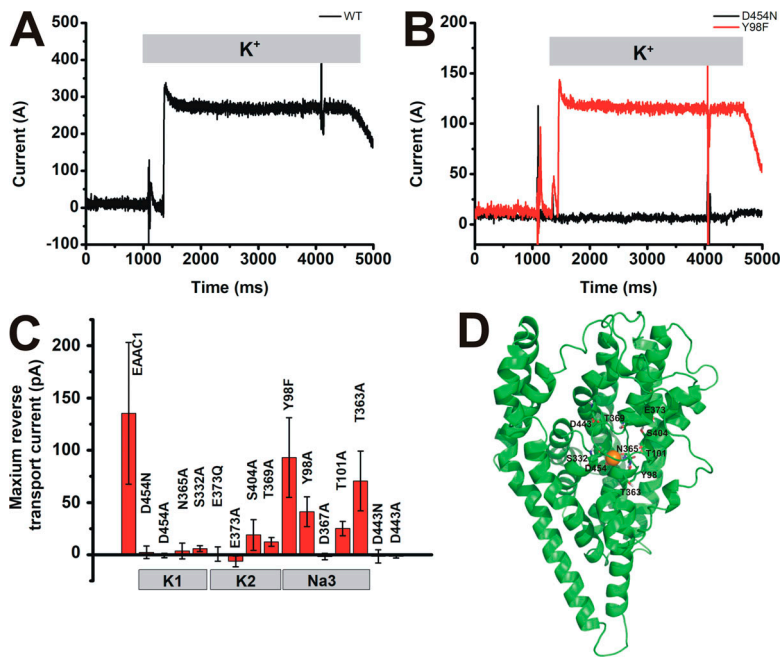
Figure 2. **Mutations to amino acid side chains predicted to coordinate K+ disrupt K+-induced reverse transport.** Whole-cell current recording experiments were performed under reverse transport conditions (130 mM NaMes and 5 mM Glu⁻ in the pipette solution; extracellular solution was switched from NMGMes to KMes [both 140 mM, indicated by gray bar]) to induced reverse transport at V = 0 mV. **(A)** Reverse transport current in EAAC1$_{WT}$. **(B)** Typical reverse transport current for EAAC1$_{Y98F}$ (red) and EAAC1$_{D454N}$ (black). Maximum of reversed transport current of all mutants shown in C. Error bars represent SD. The locations of the mutated amino acids are illustrated in D.

glutamate to the wild-type transporter and EAAC1$_{D454N}$ are shown in Fig. 4, A and B. These currents are inwardly directed, due to the outflow of internal SCN⁻, caused by the population of an anion conducting state that is kinetically located on the translocation pathway. Interestingly, outward current was observed in exchange mode in the EAAC1$_{D454A}$ transporter (Fig. 4 C), indicating that glutamate behaves like a competitive inhibitor, binding to the transporter, but being unable to induce glutamate translocation. Na⁺ and glutamate-induced exchange currents were also present in seven other mutant transporters, as shown in Fig. 4, F and I. In contrast, exchange anion current was virtually eliminated by mutations to six positions (D367A, D444N, D443A, N365A, T363A, and S332A), indicating that glutamate is either unable to bind, or binds, but cannot activate anion current in these mutant transporters.

The EAAC1$_{D454N}$ transporter, with a conservative mutation in the potential K1-site, does not catalyze K⁺-induced reverse transport current, but displays current in homoexchange mode. Together with data from a previous study (Mwaura et al., 2012),

this raises the possibility that steps associated with glutamate translocation are operational after the D454N mutation. To test this possibility, we applied extracellular glutamate in the forward transport mode. As shown in Fig. 4 B, transient anion current was still observed, but no steady-state anion current was present. The transient anion current observed in forward transport mode (K⁺ internal) is typical for mutant transporters, in which the K⁺-induced relocation step and/or internal K⁺ binding is/are impaired (Grewer et al., 2003). Upon external glutamate application, the transporter transiently visits anion conducting state(s) associated with the Na⁺/glutamate translocation reaction(s). Once the outward- to inward-facing transition is complete, the transporter gets locked in the inward-facing K⁺-bound (or *apo*) state, but it cannot complete the full transport cycle. Similar observations of transient anion current have been made previously in the wild-type transporter in the presence of low intracellular [K⁺] (Grewer et al., 2000). These results support the data from homoexchange current recordings, namely that intermediates on the translocation pathway, which are
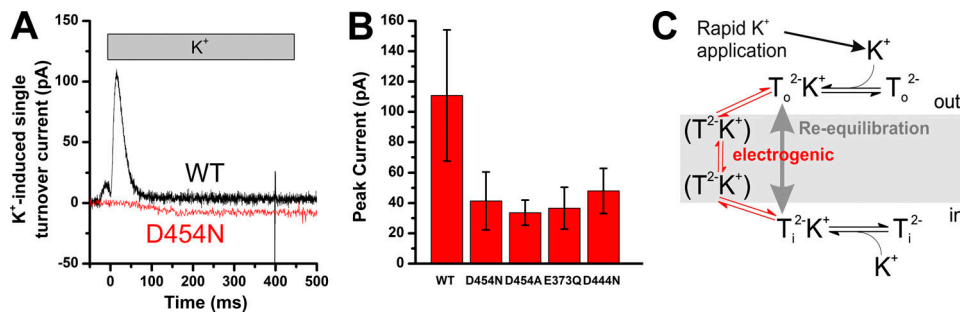

Figure 3. **K⁺ binding induced transient current signal.** **(A)** Transient current induced by the application of extracellular K⁺ (140 mM, gray bar) to the wild-type (black trace) and D454N glutamate transporter (red trace) in a single-turnover K⁺-exchange experiment (only K⁺ inside). **(B)** Comparison of select mutants' results. Error bars represent SD. **(C)** Conceptual illustration of the single-turnover K⁺-exchange experiment shown in A. Proposed electrogenic steps that are responsible for the transient charge movement are indicated in red.
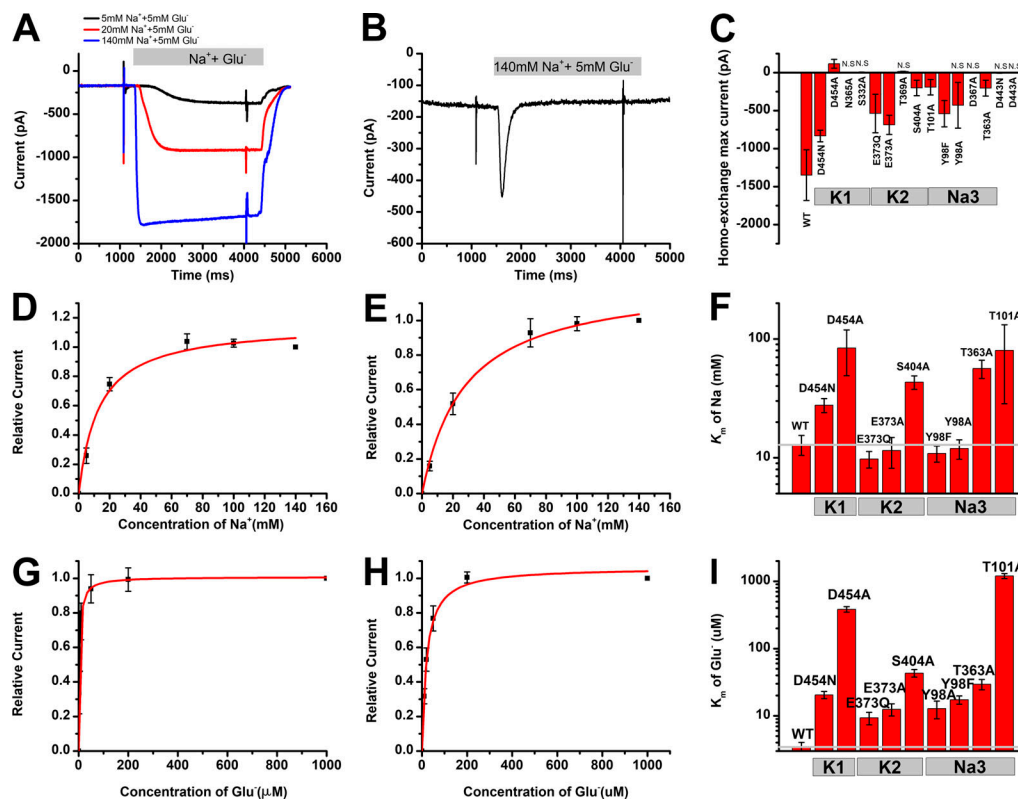
Figure 4. **Effects of K-site mutations on homoexchange and apparent Na+ and glutamate affinities.** Whole-cell current recordings were performed to test the apparent affinity of Na+/glutamate for all mutant transporters. **(A)** Typical Na+/Glu−-induced EAAC1$_{D454N}$ anion current, tested under forward transport conditions. Glutamate concentration was saturating (2.5 mM) outside, with 130 mM KSCN inside. Duration of Na+/glutamate application is indicated by the gray bar. **(B)** Transient anion current was observed in EAAC1$_{D454N}$ when switching the external solution from NMG+ to 140 mM Na+/5 mM glutamate (gray bar) in the forward transport mode. The internal solution contained KSCN. **(C)** Anion currents in homoexchange mode are compared for mutant transporters in the predicted K+-binding sites. **(D–F)** The Na+ apparent K_m was determined as 12.9 ± 2.5 mM for EAAC1$_{WT}$ (D) and 27.6 ± 3.8 mM for EAAC1$_{D454N}$ (E); Na+ apparent affinity for the K+ binding site mutant transporters is shown in F. **(G and H)** The K_m for glutamate under homoexchange conditions was determined from dose–response curves as 3.4 ± 0.6 μM for EAAC1$_{WT}$ (G) and 20.5 ± 2.5 μM for EAAC1$_{D454N}$ (H). **(I)** Glutamate K_m summary for all mutant transporters. In all experiments, the transmembrane potential was 0 mV, and error bars represent SD.

anion conducting, are still accessible in the D454N mutant transporter, but forward transport is impaired because of a defect in the K+-induced relocation reaction.

For the mutant transporters, in which K+-dependent reverse transport was blocked but homoexchange was functional, we determined apparent affinities for Na+ to test for a potentially overlapping Na+/K+ site. Typical dose–response curves for Na+ are shown in Fig. 4 (D and E) for wild-type and D454N mutant transporters. The K_m of EAAC1$_{D454N}$ for Na+ was 28 ± 4 mM (Fig. 4 E) and was increased only to a small extent compared with the wild-type transporter (K_m 13 ± 2 mM; Fig. 4 D). K_m values for Na+ for mutations to other side chains are shown in Fig. 4 F. Interestingly, mutation of E373 (Q or A) in the potential K2 site had no effect on apparent Na+ affinity, while mutations to S404 and T369 slightly decreased affinity by a factor of ∼2, suggesting that none of these amino acid side chains contribute to Na+ binding, consistent with current models of the location of the Na1–Na3 sites in EAATs (Bastug et al., 2012; Boudker et al., 2007). For the K1-site mutations, N365A was inactive, making it impossible to determine the K_m for Na+. The D454A mutation K_m for Na was 84 ± 35 mM.

Finally, we also tested the apparent glutamate affinities for the wild-type and mutant transporters. The K_m values were 3.4 ±

0.6 μM for EAAC1$_{WT}$ (Fig. 4 G), and 20.5 ± 2.5 μM for EAAC1$_{D454N}$ (Fig. 4 H). The K_m values for several mutant transporters with mutations to the potential K1 and K2 sites are summarized in Fig. 4 I, showing significant effects on apparent substrate affinity, as expected for mutations close to the substrate-binding site, as well as to the Na1 site, which in turn reduces glutamate affinity by interfering with Na+ binding.

QM calculations of cation selectivity of the K1/Na1 site

Because of the importance of the D454 position in the coordination of cations, we used QM analysis to calculate the free energy in different cation-bound states to explain the effects of neutralization of D454 through mutagenesis on K+ and Na+ binding. Binding states were mimicked using five highly conserved amino acids in the K1/Na1 site (Fig. 5, A–D). The ligands to the central metal ion included the side chains of D454, S332, and N365, in addition to the main-chain carbonyls of N451 and G361. QM calculations were performed on gas-phase models mimicking four different configurations: WT-K+ (Fig. 5 A), D454N-K+ (Fig. 5 B), WT-Na+ (Fig. 5 C), and D454N-Na+ (Fig. 5 D). Further details are provided in Materials and methods.
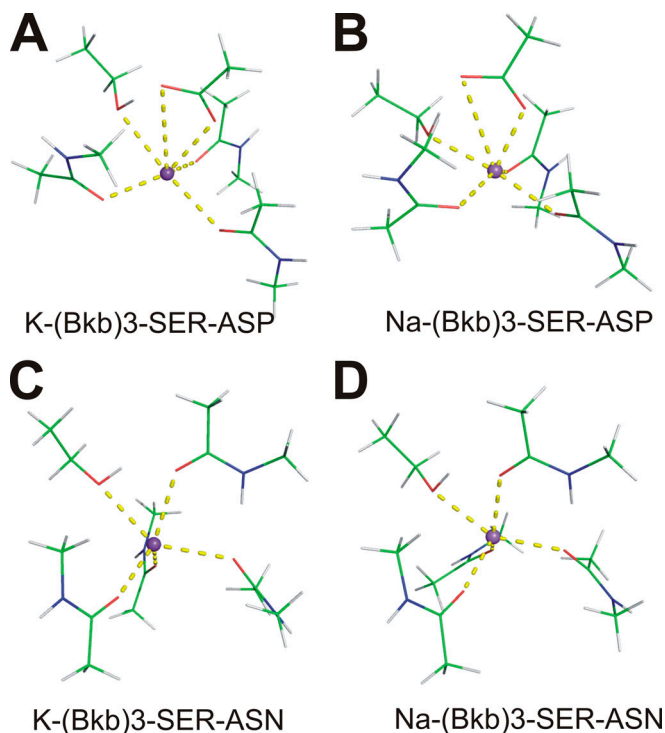
Figure 5. Gas-phase models used for QM investigations of the effect of charge neutralization on K$^+$ and Na$^+$ binding. ASN resulting from the mutation of ASP is modeled as N-methylacetamide (CH$_3$CONHCH$_3$, Bkb) as in MacKerell et al., 1998.

The QM calculations in combination with the experimental data provide insights into the geometrical features of the K1/Na1 binding site that make it more favorable toward K$^+$ binding than Na$^+$ binding. In the gas-phase models, the ligands are free to reorganize themselves around the central metal ion and form a tight coordination sphere around it. This is evident from Table S2, which shows that the K$^+$-ligating atom distances are 0.3–0.4 Å longer than the Na$^+$-ligating atom distances, consistent with K$^+$ having an ionic radius ~0.36 Å larger than that of Na$^+$. Thus, Na$^+$ is capable of accommodating the five ligands around it, if the ligands are free enough to move. Free energy calculations reveal that the increase in metal binding free energy upon charge neutralization (D to N mutation) is larger for Na$^+$ by ~5 kcal/mol than for K$^+$. This is expected from the shorter Na$^+$-ligand distances. However, electrophysiology experiments (Tao et al., 2006; Wang et al., 2019) indicate that the D454N mutation in the protein has a stronger effect on K$^+$ binding than on Na$^+$ binding, which is in contrast to gas-phase results.

A possible cause of the discrepancy could be that the amino acid side chains and backbones in the K1/Na1 site have the arrangement and flexibility to form a snug coordinate sphere around a K$^+$ ion, but not around a Na$^+$ ion. In the protein environment, the larger Na$^+$-ligand distances and the tight coordination of K$^+$ by the ligands could lead to a greater effect of charge neutralization on K$^+$ binding than on Na$^+$ binding. However, MD simulations of the protein show that this is not the case. The average ligand oxygen distances from the cation in the K$^+$ MD simulations were 3.02 Å (EAAT3) and 3.01 Å (EAAT1)

compared with 2.9 Å in the QM model. This compares to 2.6 Å (MD, EAAT3) and 2.54 Å (QM) with Na$^+$, showing that the O atom distances to the central cation are reduced with Na$^+$ compared with K$^+$ in both QM and MD simulations. Hence, the weaker Na$^+$ binding than K$^+$ binding at the Na1/K1 site in the protein environment may be due to faster kinetics associated with Na$^+$ binding/unbinding rather than weaker energetics of Na$^+$ binding.

The K1-site D454A mutation is the only mutation that blocks the K$^+$-binding step

It is important to note that interpretation based on steady-state forward or reverse transport current is not sufficient to demonstrate the effect of cation-binding site mutations on K$^+$ interaction with the transporter. For example, it is possible that a mutation blocks the conformational change associated with relocation of the K$^+$-bound transporter but does not block K$^+$ binding. Such a mutant transporter would not exhibit transport or reverse transport current. The result may be misinterpreted as the mutated residue contributing to a K$^+$ binding site, when the binding site is, in fact, still intact. To distinguish the K$^+$ binding site effects from effects on relocation, we applied a solution exchange method in homoexchange mode, switching from Na$^+$/Glu$^-$ to K$^+$ containing solution (Fig. 6). By increasing the K$^+$ concentration, the transporter binding state was successively converted by competition from the fully Na$^+$/Glu bound state, TNaGlu, to the K$^+$-bound state, TK (principle of the method illustrated by the mechanism in Fig. 6 A). Since in the TK state anion conductance is lower compared with the Na$^+$/ Glu$^-$-bound state, the anion current decreases, allowing the determination of the apparent K_m for K$^+$. Importantly, this assay can be used for mutant transporters, in which the K$^+$-relocation step is blocked, thus not eliciting steady-state transport or reverse transport current.

In agreement with these expectations, K$^+$ blocked the Na$^+$/ Glu$^-$-induced anion currents in EAAC1$_{WT}$ (Fig. 6 C), with an apparent K_m for K$^+$ of 27 ± 2 mM. When testing other potential K-site mutant transporters, Na$^+$/Glu$^-$-dependent anion conductance was affected to varying extents, showing varying K_m values compared with wild-type EAAC1 (Fig. 6 D). It is worth mentioning that based on different Na$^+$ K_m values for mutant transporters, we used Na$^+$/Glu$^-$ concentrations that generate comparable fractional populations of TNaGlu at 30–40% to keep consistent conditions for measuring the K$^+$-binding effect. Importantly, most K-site mutations did not fully eliminate K$^+$ binding, except for the K1-site mutation D454A. Other mutations that had an ~10-fold increase in K_m for K$^+$ were the Na3-site mutations Y98F and T101A (close to the K1 site) and the K2-site mutations at position E373.

Discussion

The results presented here provide further evidence for the structural basis for the interaction of K$^+$ with glutamate transporters, as well as the mechanism of K$^+$ interaction. The major findings are the following: (1) Two potential K$^+$ binding sites, K1 and K2, are predicted from MD simulations showing
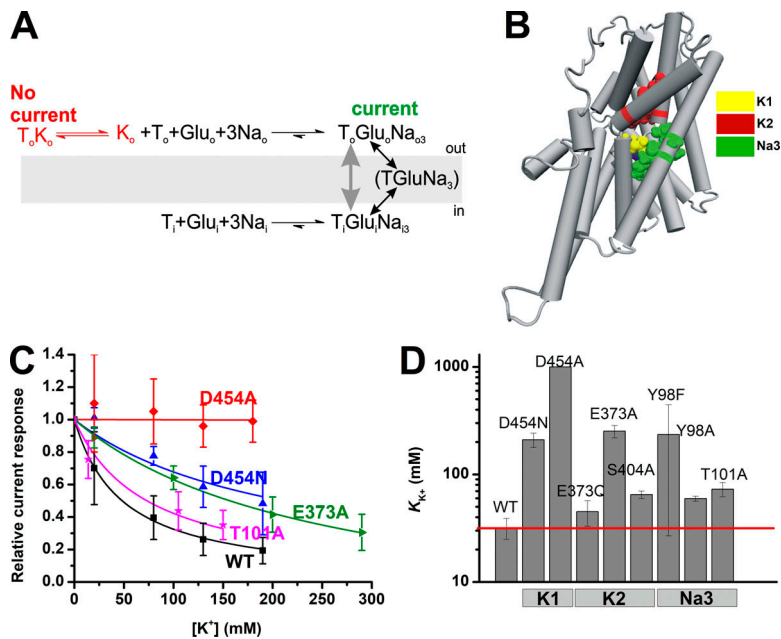
Figure 6. **Mutants blocking the translocation step but not binding steps.** Anion currents were activated under homo-exchange conditions, extracellular 10 mM Na⁺ and 5 mM glutamate, intracellular solutions contained 130 mM NaSCN and 5 mM glutamate. Subsequently, we applied K⁺ through solution exchange to inhibit steady-state anion current. **(A)** Illustrated concept of the method. **(B)** Location of the tested amino acid residues shown in three different according to contribution to K1, K2, and Na3 sites. **(C)** EAAC1$_{WT}$ and mutants' steady-state anion current as a function of K⁺ concentration. **(D)** K⁺ apparent affinity for mutant transporters determined from the dose–response curves shown in C. In C and D, error bars represent SD.

spontaneous K⁺ association. (2) K⁺ ions are stable in these binding sites for 100s of nanoseconds and often longer. (3) Mutations of most amino acid residues predicted to participate in K⁺ binding result in a transporter that is deficient in K⁺-induced reverse glutamate transport. (4) The K1 site, which is deeply buried within the membrane, overlaps with the Na1 site, and mutations to this site result in largely inactive transporters. (5) Mutations to the K2 site, which is located under HP2, reduce the affinity of, but do not abolish, K⁺ interaction with the transporter. (6) Only one mutation, namely D454A in the K1 site, results in a transporter that is unable to bind K⁺. (7) It is likely that the K1 site is responsible for binding of the K⁺ ion that induces the relocation reaction of the glutamate-free transporter. (8) The possibility of a regulatory K⁺ binding site has to be considered. Overall, these findings add to previously published evidence for the location of the K⁺ binding site (Kanner and Bendahan, 1982; Kavanaugh et al., 1997; Mwaura et al., 2012), which has not yet been identified in crystal structures of mammalian glutamate transporters, or archaeal and bacterial homologues.

K⁺/Na⁺ share the Na1/K1 binding site

Here, we used MD simulations, QM calculations, and electrophysiological analysis of mutant transporters to focus on two potential K⁺ binding positions, the Na1/K1 site, being coordinated by the side chains of D454, S332, and N365, all highly conserved within the mammalian EAAT family. The K1-site position was first proposed based on the fact that mutations to position D454 in EAAC1 abolish steady-state substrate transport (Teichman et al., 2009), as well as stimulation of currents by external application of K⁺ (Mwaura et al., 2012). However, based on these previous data, the possibility cannot be excluded that mutations to this position interfere with steps in the transport cycle other than K⁺ binding. In fact, it was shown in another report that the conservative D454N mutation had surprisingly

little effect on glutamate translocation and substrate/Na⁺ binding (Mwaura et al., 2012). In addition, the D454N mutant transporter was still able to bind K⁺ from the extracellular side, but with somewhat reduced affinity (Mwaura et al., 2012). Therefore, the evidence from previous reports on the involvement of the D454 side chain in K⁺ binding was not fully conclusive. Here, we directly show spontaneous association of K⁺ with the proposed K1 binding site in microsecond-level MD simulations, as well as a more dramatic effect of the D454A mutation on transporter function, K⁺-induced relocation, as well as full inhibition of the ability of K⁺ to bind to the mutant transporter from the extracellular side. Together with the virtual abolishment of EAAC1 function by the second K1-site mutation in position N365, these data provide more conclusive evidence that these residues are involved in actual K⁺ binding and not just the conformational change associated with relocation of the K⁺-bound transporter.

The results from experimental and computational approaches shown in this report indicate that the shared Na1/K1 site has a stronger binding affinity for K⁺ than for Na⁺. This conclusion is supported by longer residency times of K⁺ than Na⁺ in MD simulations. Here, together with a previous report (Tao et al., 2006), EAAC1$_{D454N}$ does not show a large effect on Na⁺ binding or glutamate binding/anion conductance (data not shown). In addition, apparent affinity of wild-type EAAC1 for external K⁺ is higher than that for Na⁺. Together, these results suggest that the K1/Na1 site has a slight preference for K⁺ over Na⁺.

In contrast to the Na1/K1 site, we did not obtain direct evidence for interaction of K⁺ with the previously proposed Na3 site (Bastug et al., 2012; Tao et al., 2006), which includes several highly conserved amino acid residues, including D367 and T101. While activity of the D367 mutant transporter was not high enough to test for external K⁺ binding, inhibition of exchange current by K⁺ was observed for EAAC1$_{T101A}$. The apparent K_m for

K+ was increased by a factor of ~2.5 compared with the wild-type transporter, but K+ binding was not abolished, as in the D454A mutant transporter. Similar results were obtained for the Y98 mutations, which are close to the predicted Na3 and Na1/K1 sites. Together with the lack of spontaneous binding of K+ to the Na3 site in MD simulations, we propose that the Na3 site is somewhat selective for Na+ over K+.

Interestingly, it was recently proposed that Na+ and K+ can bind simultaneously to the glutamate transporter (Wang et al., 2019). Together with the results presented here, this raises the possibility that the Na3 site can be occupied with Na+ while still allowing K+ binding to the K1 site, the K2 site, or both.

Two potential K+ binding sites
Interestingly, the MD simulation results point to the existence of a second K+ site, termed the K2 site. This site is different from any of the proposed Na+ binding sites but is in close proximity of the substrate-binding site, closed off from the extracellular solution by HP2. Side chains from conserved amino acid residues E373 and S404 contribute to this potential site (Fig. 1 B). Interestingly, K+ can still bind to the transporter after mutations to both of these sites, although with significantly reduced affinity in EAAC1$_{E373A}$. However, the more conservative E373Q mutation does not significantly alter apparent K+ affinity, suggesting that the K2 site is probably not responsible for K+-induced relocation of the glutamate-free transporter. The possibility of K+ binding to the K2-site, however, is in agreement with previous proposals based on valence screening, showing a position of favorable valence for K+ binding under HP2 (Holley and Kavanaugh, 2009). In addition, E373 has been implicated in K+ binding in early mutagenesis studies by the Kanner group (Kavanaugh et al., 1997). The K2 site being involved in relocation would be an elegant hypothesis, because E373 is thought to be the proton acceptor for H+ cotransport (Grewer et al., 2003). Thus, the K2 site could serve as a H+/K+ exchange site that would provide charge balance in both the translocation and relocation steps. While our mutagenesis results do not fully support this hypothesis, additional experiments and simulations would need to be performed to disprove it (e.g., testing of K+ affinities for association from the intracellular side). It should be noted that E373 was deprotonated in the majority of our MD simulations. However, when E373 was protonated, K+ binding to the K2 site was not observed in MD simulations. This result is in agreement with experimental results based on the E373A mutation, which mimics the protonated transporter (Grewer et al., 2003).

Which site is responsible for K+-dependent relocation?
Overall, our results suggest that the K1-site is responsible for K+-dependent relocation. This interpretation is based on the fact that the D454A mutation had the most significant effect on K+ binding (it fully abolished it both in experiment and computation; Table S1), as well as relocation (the mutation is defective in transient charge movement in K+ exchange). This interpretation is consistent with previous suggestions that this site is an overlapping binding site for Na+ and K+ (Teichman et al., 2009). Therefore, the mechanistic conclusion is that this binding site is involved in the Na+/K+ exchange mechanism of the transporter.

Previous results showed that the K1/Na1 site may be involved in charge compensation important for the functioning of the transporter, because the positive charge of the cotransported Na+ ions has to be at least partially compensated by negative charge for translocation to operate properly (Mwaura et al., 2012; Rosental et al., 2011; Watzke et al., 2001). The possibility was also raised that the D454 side chain is protonated at physiological pH. The results presented here do not provide further insight into these possibilities.

However, it should be noted that the existing experimental evidence is still conflicting with respect to the K1 site being the main K+ binding site. The major issue is that the Na1/K1 site is conserved between mammalian EAATs and Glt$_{Ph}$. In contrast to EAATs, Glt$_{Ph}$ does not require K+ countertransport for substrate uptake. An explanation was provided by Kortzak et al. (2019), who showed that K+ was able to interact with Glt$_{Ph}$ but was not needed for substrate uptake. However, the fluorescent changes upon K+ application were small and required high K+ concentrations. In another report, K+ was unable to compete with Tl+, which binds to the Na1 site, for binding to Glt$_{Ph}$ (Boudker et al., 2007). This finding is unexpected if K+ could bind to the Glt$_{Ph}$ Na1 site. In contrast, Tl+ was able to substitute for K+ in EAAT3 (Tao et al., 2008), catalyzing relocation of the glutamate-free transporter, although with much lower transport rate than K+. A possible explanation for these conflicting results is that the Na1 site has different cation selectivity in Glt$_{Ph}$ and EAATs, despite the conserved nature of the amino acid side chains contributing to the site. It can be speculated that this difference in selectivity is caused by secondary structural factors other than the primary cation ligand sphere, restricting the flexibility/size of this site in Glt$_{Ph}$, making it unable to adopt K+.

Effects of mutations on K+-dependent relocation rather than K+ binding
Previous attempts to identify the location of the K+ site of glutamate transporters were based mainly on current recording and transport assays under steady-state conditions (Kavanaugh et al., 1997). In these experiments, mutant transporters were tested for the ability of K+ to induce relocation to complete the transport cycle. While the results from these experiments are important, it should be noted that many mutations block the K+-dependent relocation step, even though they may not be directly involved in K+ binding, and thus do not contribute to the K+ binding site. Therefore, it is critical to be able to differentiate between a mutant's effect on binding versus relocation (i.e., conformational changes of the transporter). For example, E373 mutations result in block of the K+-dependent relocation step, but not K+ binding (Grewer et al., 2003; Kavanaugh et al., 1997; Watzke et al., 2001). Our work presented here improves on these earlier results in two ways: (1) Our assay to test for inhibition of Na+/glutamate homoexchange activity by external K+ (Fig. 6) allows for direct determination of apparent K+ affinity. Several mutations that were previously thought to be defective in K+ interaction still show K+ inhibition in this assay. (2) The ability to test for transient charge movements in the K+/K+ exchange mode. This technique allows the isolation of the relocation step in the transport cycle. Overall, application of these

methods sheds additional light on the mechanism of K⁺ interaction with mutant transporters, and they may be useful for further mutagenesis studies.

Conclusions

In summary, we have shown evidence for spontaneous binding of K⁺ to two potential binding sites in MD simulations. The two binding sites were experimentally tested using site-directed mutagenesis, suggesting that the K1 site is shared with the Na1 site, with slight preference for K⁺ binding. Mutations to this site had the most significant effect on K⁺ binding/relocation. This is the site most likely responsible for K⁺-induced relocation of the glutamate-free transporter. In contrast, the K2 site, which is located under HP2, seems to be less sensitive to mutagenesis, possibly indicating a regulatory function for this site.

While this work was under preparation, a paper was published describing the identification of K⁺ binding sites in glutamate transporters from MD simulations, including the K1/Na1 site and K2 site (Kortzak et al., 2019), as well as two additional predicted K⁺ binding sites, which were not seen in our work. However, while K⁺ affinities were calculated based on simulation, no experimental information on affinities was provided for the wild-type binding sites, as well as for mutant transporters. Thus, our work presented here provides new information and expands on the characterization of these binding sites in addition to what was presented by Kortzak et al. (2019). However, the major conclusion (i.e., that the K1 site is likely responsible for the K⁺-induced conformational changes [relocation]) is the same in the work from the Fahlke group (Kortzak et al., 2019) and our work presented here. Furthermore, while under review, an EAAT3 crystal structure was published as a preprint (Qiu et al., 2020 *Preprint*).

Acknowledgments

References

Arkhipova, V., A. Guskov, and D.J. Slotboom. 2020. Structural ensemble of a glutamate transporter homologue in lipid nanodisc environment. *Nat. Commun.* 11:998. https://doi.org/10.1038/s41467-020-14834-8

Bastug, T., G. Heinzelmann, S. Kuyucak, M. Salim, R.J. Vandenberg, and R.M. Ryan. 2012. Position of the third Na+ site in the aspartate transporter GltPh and the human glutamate transporter, EAAT1. *PLoS One.* 7. e33058. https://doi.org/10.1371/journal.pone.0033058

Bendahan, A., A. Armon, N. Madani, M.P. Kavanaugh, and B.I. Kanner. 2000. Arginine 447 plays a pivotal role in substrate interactions in a neuronal glutamate transporter. *J. Biol. Chem.* 275:37436–37442. https://doi.org/10.1074/jbc.M006536200

Bergles, D.E., A.V. Tzingounis, and C.E. Jahr. 2002. Comparison of coupled and uncoupled currents during glutamate uptake by GLT-1 transporters. *J. Neurosci.* 22:10153–10162. https://doi.org/10.1523/JNEUROSCI.22-23-10153.2002

Boudker, O., R.M. Ryan, D. Yernool, K. Shimamoto, and E. Gouaux. 2007. Coupling substrate and ion binding to extracellular gate of a sodium-dependent aspartate transporter. *Nature.* 445:387–393. https://doi.org/10.1038/nature05455

Canul-Tec, J.C., R. Assal, E. Cirri, P. Legrand, S. Brier, J. Chamot-Rooke, and N. Reyes. 2017. Structure and allosteric inhibition of excitatory amino acid transporter 1. *Nature.* 544:446–451. https://doi.org/10.1038/nature22064

Dudev, T., K. Mazmanian, and C. Lim. 2018. Competition between Li⁺ and Na⁺ in sodium transporters and receptors: Which Na⁺-Binding sites are "therapeutic" Li⁺ targets? *Chem. Sci. (Camb.).* 9:4093–4103. https://doi.org/10.1039/C7SC05284G

Frisch, M.J. G.W. Trucks, H.B. Schlegel, G.E. Scuseria, M.A. Robb, J.R. Cheeseman, G. Scalmani, V. Barone, G.A. Petersson, H. Nakatsuji, et al. 2016. Gaussian 09. Gaussian, Inc., Wallingford, CT.

Garaeva, A.A., A. Guskov, D.J. Slotboom, and C. Paulino. 2019. A one-gate elevator mechanism for the human neutral amino acid transporter ASCT2. *Nat. Commun.* 10:3427. https://doi.org/10.1038/s41467-019-11363-x

Grewer, C., N. Watzke, M. Wiessner, and T. Rauen. 2000. Glutamate translocation of the neuronal glutamate transporter EAAC1 occurs within milliseconds. *Proc. Natl. Acad. Sci. USA.* 97:9706–9711. https://doi.org/10.1073/pnas.160170397

Grewer, C., N. Watzke, T. Rauen, and A. Bicho. 2003. Is the glutamate residue Glu-373 the proton acceptor of the excitatory amino acid carrier 1? *J. Biol. Chem.* 278:2585–2592. https://doi.org/10.1074/jbc.M207956200

Grewer, C., Z. Zhang, J. Mwaura, T. Albers, A. Schwartz, and A. Gameiro. 2012. Charge compensation mechanism of a Na+-coupled, secondary active glutamate transporter. *J. Biol. Chem.* 287:26921–26931. https://doi.org/10.1074/jbc.M112.364059

Guskov, A., S. Jensen, I. Faustino, S.J. Marrink, and D.J. Slotboom. 2016. Coupled binding mechanism of three sodium ions and aspartate in the glutamate transporter homologue Glt_Tk. *Nat. Commun.* 7:13420. https://doi.org/10.1038/ncomms13420

Hanwell, M.D., D.E. Curtis, D.C. Lonie, T. Vandermeersch, E. Zurek, and G.R. Hutchison. 2012. Avogadro: an advanced semantic chemical editor, visualization, and analysis platform. *J. Cheminform.* 4:17. https://doi.org/10.1186/1758-2946-4-17

Harvey, M.J., G. Giupponi, and G.D. Fabritiis. 2009. ACEMD: Accelerating Biomolecular Dynamics in the Microsecond Time Scale. *J. Chem. Theory Comput.* 5:1632–1639. https://doi.org/10.1021/ct9000685

Heinzelmann, G., and S. Kuyucak. 2014. Molecular dynamics simulations elucidate the mechanism of proton transport in the glutamate transporter EAAT3. *Biophys. J.* 106:2675–2683. https://doi.org/10.1016/j.bpj.2014.05.010

Heinzelmann, G., T. Baştuğ, and S. Kuyucak. 2011. Free energy simulations of ligand binding to the aspartate transporter Glt(Ph). *Biophys. J.* 101:2380–2388. https://doi.org/10.1016/j.bpj.2011.10.010

Holley, D.C., and M.P. Kavanaugh. 2009. Interactions of alkali cations with glutamate transporters. *Philos. Trans. R. Soc. Lond. B Biol. Sci.* 364:155–161. https://doi.org/10.1098/rstb.2008.0246

Humphrey, W., A. Dalke, and K. Schulten. 1996. VMD: visual molecular dynamics. *J. Mol. Graph.* 14:33–38–28. https://doi.org/10.1016/0263-7855(96)00018-5

Jensen, S., A. Guskov, S. Rempel, I. Hänelt, and D.J. Slotboom. 2013. Crystal structure of a substrate-free aspartate transporter. *Nat. Struct. Mol. Biol.* 20:1224–1226. https://doi.org/10.1038/nsmb.2663

Kanner, B.I., and A. Bendahan. 1982. Binding order of substrates to the sodium and potassium ion coupled L-glutamic acid transporter from rat brain. *Biochemistry*. 21:6327–6330. https://doi.org/10.1021/bi00267a044

Kavanaugh, M.P., A. Bendahan, N. Zerangue, Y. Zhang, and B.I. Kanner. 1997. Mutation of an amino acid residue influencing potassium coupling in the glutamate transporter GLT-1 induces obligate exchange. *J. Biol. Chem.* 272:1703–1708. https://doi.org/10.1074/jbc.272.3.1703

Kortzak, D., C. Alleva, I. Weyand, D. Ewers, M.I. Zimmermann, A. Franzen, J.P. Machtens, and C. Fahlke. 2019. Allosteric gate modulation confers K+ coupling in glutamate transporters. *EMBO J.* 38. e101468. https://doi.org/10.15252/embj.2019101468

Kovermann, P., M. Hessel, D. Kortzak, J.C. Jen, J. Koch, C. Fahlke, and T. Freilinger. 2017. Impaired K+ binding to glial glutamate transporter EAAT1 in migraine. *Sci. Rep.* 7:13913. https://doi.org/10.1038/s41598-017-14176-4

Machtens, J.P., D. Kortzak, C. Lansche, A. Leinenweber, P. Kilian, B. Begemann, U. Zachariae, D. Ewers, B.L. de Groot, R. Briones, et al. 2015. Mechanisms of anion conduction by coupled glutamate transporters. *Cell*. 160:542–553. https://doi.org/10.1016/j.cell.2014.12.035

MacKerell, A.D., D. Bashford, M. Bellott, R.L. Dunbrack, J.D. Evanseck, M.J. Field, S. Fischer, J. Gao, H. Guo, D. Joseph-McCarthy, et al. 1998. All-atom empirical potential for molecular modeling and dynamics studies of proteins. *J Phys Chem B*. 102:3586–3616. https://doi.org/10.1021/jp973084f

Mwaura, J., Z. Tao, H. James, T. Albers, A. Schwartz, and C. Grewer. 2012. Protonation state of a conserved acidic amino acid involved in Na(+) binding to the glutamate transporter EAAC1. *ACS Chem. Neurosci.* 3: 1073–1083. https://doi.org/10.1021/cn300163p

Phillips, J.C., R. Braun, W. Wang, J. Gumbart, E. Tajkhorshid, E. Villa, C. Chipot, R.D. Skeel, L. Kalé, and K. Schulten. 2005. Scalable molecular dynamics with NAMD. *J. Comput. Chem.* 26:1781–1802. https://doi.org/10.1002/jcc.20289

Qiu, B., D. Matthies, E. Fortea, Z. Yu, and O. Boudker. 2020. Transport mechanism of the neuronal excitatory amino acid transporter. *bioRxiv*. (Preprint posted June 2, 2020) https://doi.org/10.1101/2020.06.01.127704

Reyes, N., C. Ginter, and O. Boudker. 2009. Transport mechanism of a bacterial homologue of glutamate transporters. *Nature*. 462:880–885. https://doi.org/10.1038/nature08616

Rosental, N., A. Gameiro, C. Grewer, and B.I. Kanner. 2011. A conserved aspartate residue located at the extracellular end of the binding pocket controls cation interactions in brain glutamate transporters. *J. Biol. Chem.* 286:41381–41390. https://doi.org/10.1074/jbc.M111.291021

Studer, G., M. Biasini, and T. Schwede. 2014. Assessing the local structural quality of transmembrane protein models using statistical potentials (QMEANBrane). *Bioinformatics*. 30:i505–i511. https://doi.org/10.1093/bioinformatics/btu457

Szatkowski, M., B. Barbour, and D. Attwell. 1990. Non-vesicular release of glutamate from glial cells by reversed electrogenic glutamate uptake. *Nature*. 348:443–446. https://doi.org/10.1038/348443a0

Tanaka, K., K. Watase, T. Manabe, K. Yamada, M. Watanabe, K. Takahashi, H. Iwama, T. Nishikawa, N. Ichihara, T. Kikuchi, et al. 1997. Epilepsy and exacerbation of brain injury in mice lacking the glutamate transporter GLT-1. *Science*. 276:1699–1702. https://doi.org/10.1126/science.276.5319.1699

Tao, Z., and C. Grewer. 2005. The conserved histidine 295 does not contribute to proton cotransport by the glutamate transporter EAAC1. *Biochemistry*. 44:3466–3476. https://doi.org/10.1021/bi047812i

Tao, Z., Z. Zhang, and C. Grewer. 2006. Neutralization of the aspartic acid residue Asp-367, but not Asp-454, inhibits binding of Na+ to the glutamate-free form and cycling of the glutamate transporter EAAC1. *J. Biol. Chem.* 281:10263–10272. https://doi.org/10.1074/jbc.M510739200

Tao, Z., A. Gameiro, and C. Grewer. 2008. Thallium ions can replace both sodium and potassium ions in the glutamate transporter excitatory amino acid carrier 1. *Biochemistry*. 47:12923–12930. https://doi.org/10.1021/bi8017174

Tao, Z., N. Rosental, B.I. Kanner, A. Gameiro, J. Mwaura, and C. Grewer. 2010. Mechanism of cation binding to the glutamate transporter EAAC1 probed with mutation of the conserved amino acid residue Thr101. *J. Biol. Chem.* 285:17725–17733. https://doi.org/10.1074/jbc.M110.121798

Teichman, S., S. Qu, and B.I. Kanner. 2009. The equivalent of a thallium binding residue from an archeal homolog controls cation interactions in brain glutamate transporters. *Proc. Natl. Acad. Sci. USA*. 106: 14297–14302. https://doi.org/10.1073/pnas.0904625106

Towns, J., T. Cockerill, M. Dahan, I. Foster, K. Gaither, A. Grimshaw, V. Hazlewood, S. Lathrop, D. Lifka, G.D. Peterson, et al. 2014. XSEDE: Accelerating Scientific Discovery. *Comput. Sci. Eng.* 16:62–74. https://doi.org/10.1109/MCSE.2014.80

Verdon, G., and O. Boudker. 2012. Crystal structure of an asymmetric trimer of a bacterial glutamate transporter homolog. *Nat. Struct. Mol. Biol.* 19: 355–357. https://doi.org/10.1038/nsmb.2233

Verdon, G., S. Oh, R.N. Serio, and O. Boudker. 2014. Coupled ion binding and structural transitions along the transport cycle of glutamate transporters. *eLife*. 3. e02283. https://doi.org/10.7554/eLife.02283

Wadiche, J.I., S.G. Amara, and M.P. Kavanaugh. 1995. Ion fluxes associated with excitatory amino acid transport. *Neuron*. 15:721–728. https://doi.org/10.1016/0896-6273(95)90159-0

Wang, J., T. Albers, and C. Grewer. 2018. Energy Landscape of the Substrate Translocation Equilibrium of Plasma-Membrane Glutamate Transporters. *J. Phys. Chem. B*. 122:28–39. https://doi.org/10.1021/acs.jpcb.7b09059

Wang, J., L. Zielewicz, and C. Grewer. 2019. A K+/Na+ co-binding state: Simultaneous *versus* competitive binding of K+ and Na+ to glutamate transporters. *J. Biol. Chem.* 294:12180–12190. https://doi.org/10.1074/jbc.RA119.009421

Watzke, N., E. Bamberg, and C. Grewer. 2001. Early intermediates in the transport cycle of the neuronal excitatory amino acid carrier EAAC1. *J. Gen. Physiol.* 117:547–562. https://doi.org/10.1085/jgp.117.6.547

Yernool, D., O. Boudker, Y. Jin, and E. Gouaux. 2004. Structure of a glutamate transporter homologue from Pyrococcus horikoshii. *Nature*. 431: 811–818. https://doi.org/10.1038/nature03018

Zerangue, N., and M.P. Kavanaugh. 1996a. Flux coupling in a neuronal glutamate transporter. *Nature*. 383:634–637. https://doi.org/10.1038/383634a0

Zerangue, N., and M.P. Kavanaugh. 1996b. Interaction of L-cysteine with a human excitatory amino acid transporter. *J. Physiol.* 493:419–423. https://doi.org/10.1113/jphysiol.1996.sp021393

Zhang, Z., Z. Tao, A. Gameiro, S. Barcelona, S. Braams, T. Rauen, and C. Grewer. 2007. Transport direction determines the kinetics of substrate transport by the glutamate transporter EAAC1. *Proc. Natl. Acad. Sci. USA*. 104:18025–18030. https://doi.org/10.1073/pnas.0704570104

Zielewicz, L., J. Wang, E. Ndaru, and C.T. Grewer. 2019. Transient Kinetics Reveal Mechanism and Voltage Dependence of Inhibitor and Substrate Binding to Glutamate Transporters. *ACS Chem. Biol.* 14:1002–1010. https://doi.org/10.1021/acschembio.9b00194

Zimmermann, L., A. Stephens, S.Z. Nam, D. Rau, J. Kübler, M. Lozajic, F. Gabler, J. Söding, A.N. Lupas, and V. Alva. 2018. A Completely Reimplemented MPI Bioinformatics Toolkit with a New HHpred Server at its Core. *J. Mol. Biol.* 430:2237–2243. https://doi.org/10.1016/j.jmb.2017.12.007

Zomot, E., and I. Bahar. 2013. Intracellular gating in an inward-facing state of aspartate transporter Glt(Ph) is regulated by the movements of the helical hairpin HP2. *J. Biol. Chem.* 288:8231–8237. https://doi.org/10.1074/jbc.M112.438432

```
            ....|....| ....|....| ....|....| ....|....| ....|....|
                    10         20         30         40         50
EAAT3   MGKPARKGCE WKRFLKNNWV LLSTVAAVVL GITTGVLVRE HSNLSTLEKF
GltPh   ---------- -------YPV LIKILIGLIL GAIVGLILGH Y-GYAHAVHT


            ....|....| ....|....| ....|....| ....|....| ....|....|
                    60         70         80         90        100
EAAT3   YFAFPGEILM RMLKLIILPL IISSMITGVA ALDSNVSGKI GLRAVVYYFC
GltPh   YVKPFGDLFV RLLKMLVMPI VFASLVVGAA SISPARLGRV GVKIVVYYLL


            ....|....| ....|....| ....|....| ....|....| ....|....|
                   110        120        130        140        150
EAAT3   TTLIAVILGI VLVVSIKPGV TQKVGEIART GSTPEVSTVD AMLDLIRNMF
GltPh   TSAFAVTLGI IMARLFNPG- AGIHLAVGG- ------QQFP PLVHILLDIV


            ....|....| ....|....| ....|....| ....|....| ....|....|
                   160        170        180        190        200
EAAT3   PENLVQACFQ QYKTKREEVK PPSDPEMNMT EESFTAVMTT AISKNKTKEY
GltPh   PTNPFGAL-- ---------- ---------- ---------- ----------


            ....|....| ....|....| ....|....| ....|....| ....|....|
                   210        220        230        240        250
EAAT3   KIVGMYSDGI NVLGLIVFCL VFGLVIGKMG --------EK GQILVDFFNA
GltPh   -------ANG QVLPTIFFAI ILGIAITYLM NSENEKVRKS AETLLDAING


            ....|....| ....|....| ....|....| ....|....| ....|....|
                   260        270        280        290        300
EAAT3   LSDATMKIVQ IIMCYMPLGI LFLIAGKIIE VEDWEIFRKL GLYMATVLTG
GltPh   LAEAMYKIVN GVMQYAPIGV FALIAYVMAE QG-VHVVGEL AKVTAAVYVG


            ....|....| ....|....| ....|....| ....|....| ....|....|
                   310        320        330        340        350
EAAT3   LAIHSIVILP LIYFIVVRKN PFRFAMGMAQ ALLTALMISS SSATLPVTFR
GltPh   LTLQILLVYF VLLK-IYGID PISFIKHAKD AMLTAFVTRS SSGTLPVTMR


            ....|....| ....|....| ....|....| ....|....| ....|....|
                   360        370        380        390        400
EAAT3   CAEENNQVDK RITRFVLPVG ATINMDGTAL YEAVAAVFIA QLNDLDLGIG
GltPh   VAKE-MGISE GIYSFTLPLG ATINMDGTAL YQGVCTFFIA NALGSHLTVG


            ....|....| ....|....| ....|....| ....|....| ....|....|
                   410        420        430        440        450
EAAT3   QIITISITAT SASIGAAGVP QAGLVTMVIV LSAVGLPAE- -----DVTLI
GltPh   QQLTIVLTAV LASIGTAGVP GAGAIMLAMV LHSVGLPLTD PNVAAAYAMI


            ....|....| ....|....| ....|....| ....|....| ....|....|
                   460        470        480        490        500
EAAT3   IAVDWLLDRF RTMVNVLGDA FGTGIVEKLS KKELEQMDVS SEVNIVNPFA
GltPh   LGIDAILDMG RTMVNVTGDL TGTAIVAKTE ---------- ----------


            ....|....| ....|....| ....|....| ....|...
                   510        520        530
EAAT3   LESTILDNED SDTKKSYVNG GFAVDKSDTI SFTQTSQF
GltPh   ---------- ---------- ---------- --------
```

Figure S1. **Sequence alignment used for generating the EAAT3 homology model, in analogy to alignments presented by Yernool et al. (2004).** EAAT3 N- and C-termini, as well as the extracellular loop between positions 160 and 206 were removed.
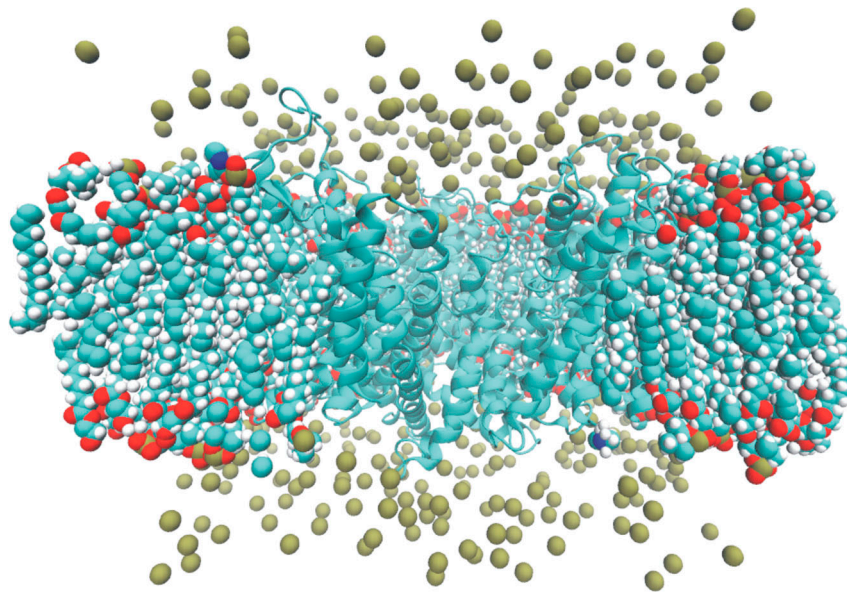
Figure S2. **Simulation environment.** Illustration of the simulation box, including the three EAAT3 subunits (ribbons in cyan) in *apo* state, as well as K$^+$ (tan spheres) ions. The lipid is shown in van der Waals representation.
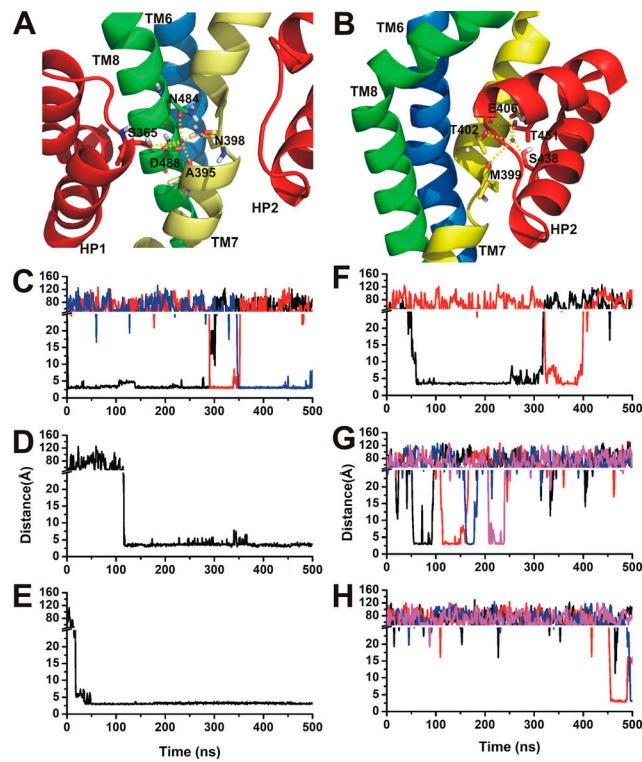

Figure S3. **MD simulations reveal potential K$^+$ binding sites in EAAT1.** MD simulations were based on EAAT1 structure (PDB accession no. 5LM4). Typical trajectories were selected and analyzed here. **(A)** K$^+$ binding at K1 site. **(B)** K$^+$ binding at K2 site. Trajectories analyzed indicated that the K$^+$ ion spontaneously binds to the K1 site (C–E), and K2 site (F–H). The calculation methods and illustrations are the same as in Fig. 1. The K$^+$ concentration was 1 M.
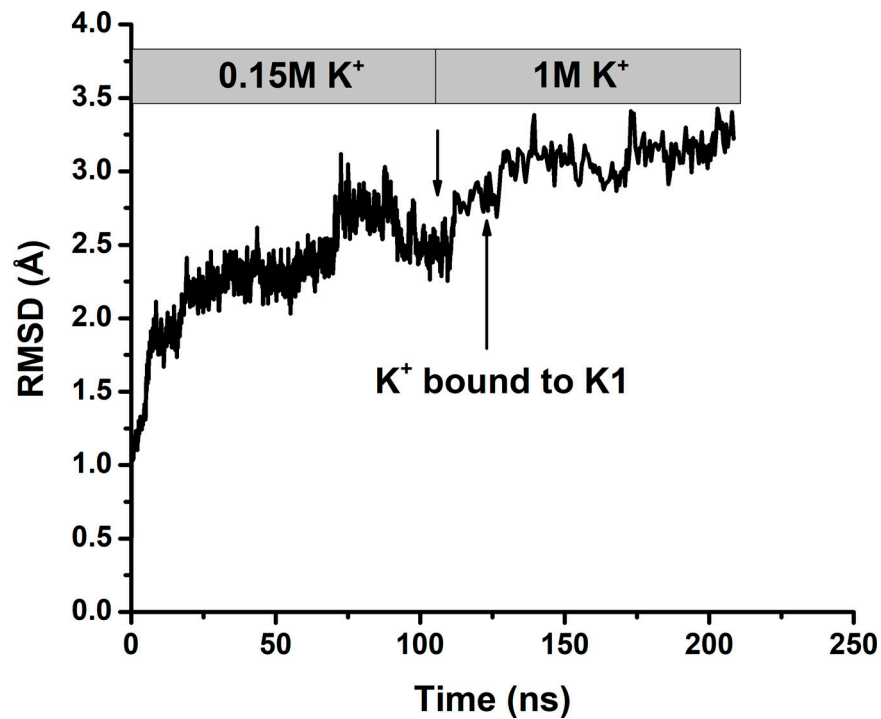
Figure S4.   **Typical RMSD plots for MD simulations before and after application of high [K⁺] show that the *apo* structure was equilibrated**. After removal of Na⁺/Asp, the EAAT3-Glt$_{Ph}$ homology model structure was used for MD runs in the 0.15 M K⁺ condition, with no binding events observed. In the first 5-ns period, a harmonic constraint of constant 0.04 was applied to the protein Cα. Constraints were then released, and the NPT simulation of the *apo* structure was allowed to equilibrate, resulting in an increase in RMSD due to a structural change of the aspartate-free structure. At the time indicated by the arrow, the K⁺ concentration was raised to 1 M. A K⁺ binding event was observed soon after, which led to only a slight change in RMSD.
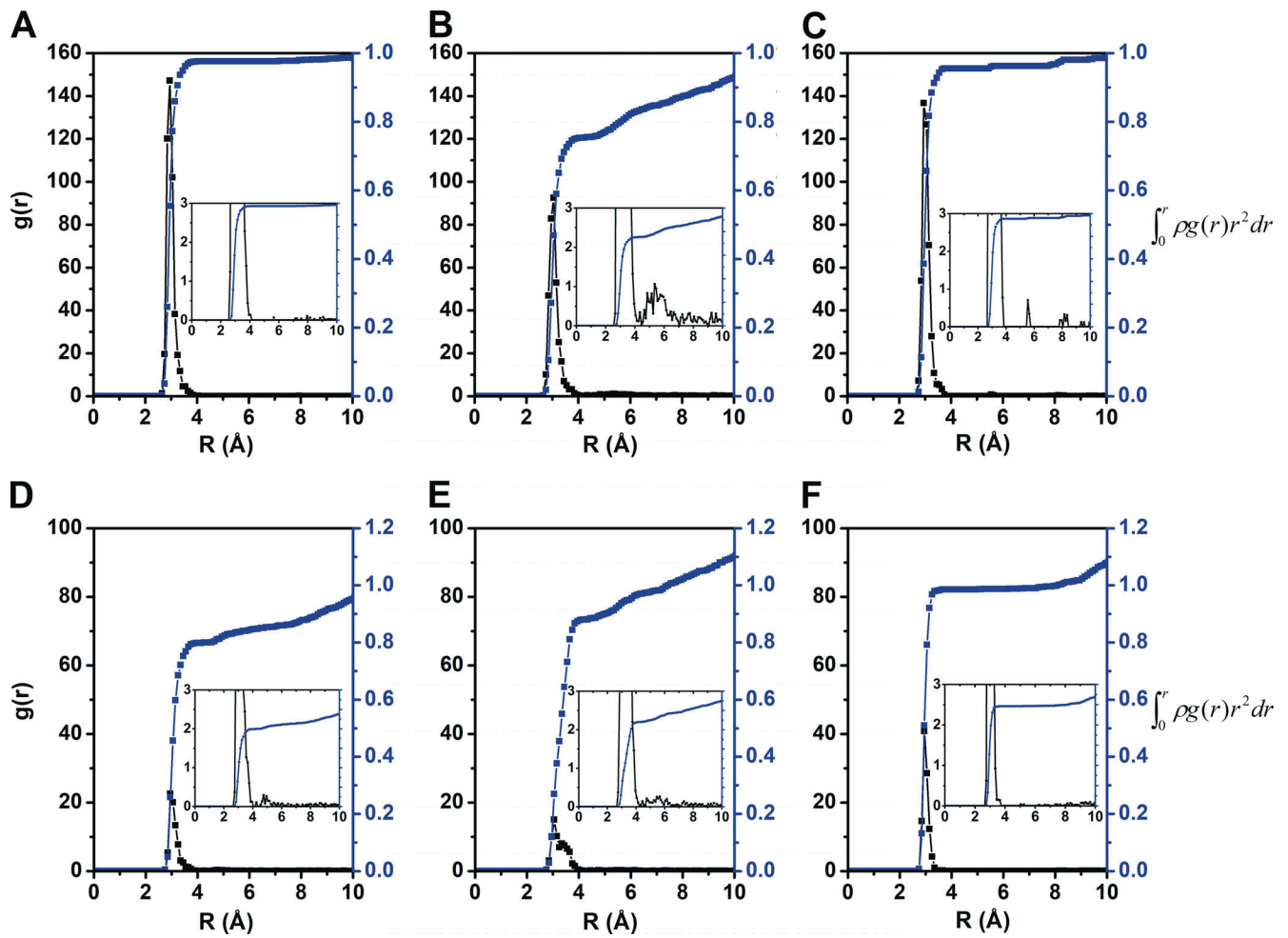
Figure S5. **K⁺ radial distribution functions from spontaneous K⁺-binding simulations. (A–C)** Radial distribution of K⁺ ions around the C_γ atom of D454 in the trajectories corresponding to Fig. 1, C–E. **(D–F)** Radial distribution of K⁺ ions around the C_δ atom of E373 in the trajectories corresponding to Fig. 1, F–H. The insets show the radial disctribution function with the y axis magnified, illustrating the small contribution to the distribution at larger distances.
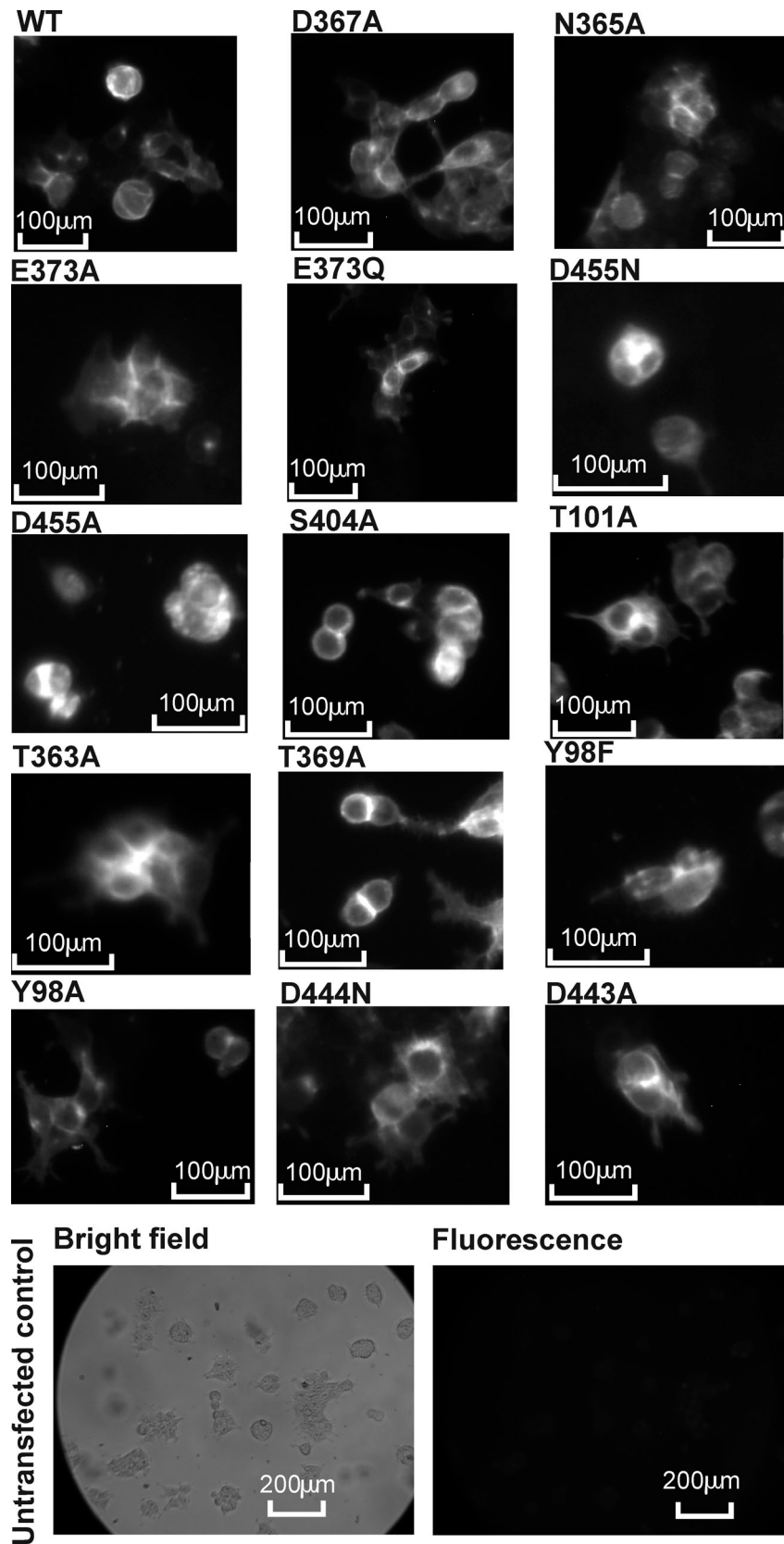
Figure S6. **EAAC1 WT and mutant expression tested using immunofluorescence microscopy.** Fluorescence micrographs of EAAC1_{WT} and mutant transporters expressing in HEK293 cells immunolabeled for EAAC1. The scale bar represents 100 µm.

Tables S1 and S2 are provided online. Table S1 shows an EAAT3 homology model based on Glt$_{Ph}$. Table S2 shows distances between the central metal ion and ligands in the QM-optimized structures of the gas-phase models.